

Cite this: *J. Mater. Chem. A*, 2021, 9, 505

High-performance all-organic aqueous batteries based on a poly(imide) anode and poly(catechol) cathode†

Nagaraj Patil, ^{ID}*^a Andreas Mavrandonakis, ^{ID}^a Christine Jérôme, ^{ID}^b Christophe Detrembleur, ^{ID}^b Nerea Casado, ^{ID}^c David Mecerreyes, ^{ID}^{cd} Jesus Palma ^{ID}^a and Rebeca Marcilla ^{ID}*^a

Aqueous all-polymer batteries (AqPBs) are foreseen as promising solutions for safe, sustainable, and high-performance energy storage applications. Nevertheless, their development is still challenging as it demands precise optimization of both electrodes and the electrolyte composition to be able to sustain a stable redox activity, while delivering an optimal voltage output. Herein, we report AqPBs based on a poly(imide) (PI) anode and poly(catechol) (PC) cathode that exhibit tunable cell voltage depending on the salt used in the aqueous electrolyte, *i.e.*, 0.58, 0.74, 0.89, and 0.95 V, respectively, when Li⁺, Zn²⁺, Al³⁺, and Li⁺/H⁺ were utilized as charge carriers. The PI–PC full-cell delivers the best rate performance (a sub-second charge/discharge) and cycling stability (80% capacity retention over 1000 cycles at 5 A g⁻¹) in Li⁺. Furthermore, a maximum energy/power density of 80.6 W h kg_{anode+cathode}⁻¹/348 kW kg_{anode+cathode}⁻¹ is achieved in Li⁺/H⁺, superior to most of the previously reported AqPBs.

Received 24th September 2020
Accepted 18th November 2020

DOI: 10.1039/d0ta09404h

rsc.li/materials-a

Introduction

The proper integration of affordable, scalable and eco-friendly electrochemical energy storage (EES) systems is critical to facilitate the development of a safe, secure, and sustainable energy landscape.^{1,2} However, commercial Li-ion batteries exclusively include insertion-type inorganic anodes, 3d transition metal cathodes and organic electrolytes, which are unsafe, scarce, expensive and energy intensive, and hardly meet the requirements of a sustainable society.³ This calls for a radical change in research and development beyond Li-ion battery chemistries to meet the ever-increasing sustainability demands.⁴

Aqueous all-polymer batteries (AqPBs) that incorporate redox-active polymers (RAPs) as organic electrode materials (OEMs) and aqueous solutions as safe and cost-effective electrolytes can be promising alternatives for the development of sustainable energy storage systems.^{5–7} Although a plethora of RAPs have been successfully applied as OEMs in numerous

rechargeable battery technologies (mostly, in metal-ion–polymer configuration),^{8–17} examples of AqPBs sporadically appeared in the literature.^{18,19} This is partly due to the formidable challenge that requires careful designing of both anode and cathode RAP partners to be not only able to sustain their redox activity in aqueous media, but also deliver a high voltage output within a relatively narrow electrochemical window of aqueous electrolytes (~1.23 and ~2 V for pure water and typical salt-in-water electrolytes, respectively).^{20–23}

Based on the charge storage mechanisms of RAPs, they can be generally classified into: n-type undergoing N ↔ N⁻, p-type undergoing P ↔ P⁺, and bipolar exhibiting B⁻ ↔ B ↔ B⁺ redox reactions, with the simultaneous shuttling of electro-neutralizing cations, anions, and dual ions, respectively.^{8–15,18,19} Depending on the RAP (n- or p-type) and the chemical nature of the charge carriers, three kinds of AqPBs were realized: (i) n|n-type combination is generally preferred for the capacity-oriented design (20–65 mA h g_{cell}⁻¹, <1 V),^{24–26} p|p-type combination mostly preferred for the voltage-oriented design (1.1–1.3 V, <45 mA h g_{cell}⁻¹),^{27–29} and n|p-type combination offers a compromise between the capacity and the voltage (10–52 mA h g_{cell}⁻¹ and 0.9–1.3 V)^{29–33} (Fig. S1 and Table S1, see the ESI†). From these limited examples, it is evident that the development of AqPBs is at a slow pace and further it is necessary to simultaneously improve their capacity and voltage in order to be competitive with other aqueous-based battery technologies.^{18,19}

Among different varieties of n-type Redox-Active Polymers (RAPs), poly(imide)s and poly(quinone)s have been attracting tremendous interest in AqPBs owing to their (i) high theoretical

^aElectrochemical Processes Unit, IMDEA Energy, Avda. Ramón de la Sagra 3, 28935 Móstoles, Madrid, Spain. E-mail: rebeca.marcilla@imdea.org; nagaraj.patil@imdea.org

^bCentre for Education and Research on Macromolecules (CERM), CESAM Research Unit, Department of Chemistry, University of Liege, Allée de la Chimie B6A, 4000 Liège, Belgium

^cPOLYMAT, University of the Basque Country UPV/EHU, Joxe Mari Korta Center, Avda. Tolosa 72, 20018 Donostia-San Sebastián, Spain

^dIkerbasque, Basque Foundation for Science, E-48011, Bilbao, Spain

† Electronic supplementary information (ESI) available: ESI Table, computational procedure and figures. See DOI: 10.1039/d0ta09404h



number of electrons exchange per unit of catechol/*o*-quinone ($n = 2$), and w_{RA} and MW_{RA} are the weight fraction and the molecular weight of redox-active (RA) units, respectively.⁴² The theoretical specific capacity of PC and PI is about 180 and 166 mA h g⁻¹, respectively. The energy density (W h kg⁻¹) of the full-cell was determined by integrating the area under the galvanostatic specific capacity_{anode+cathode}-voltage discharge profiles. Power density (W kg⁻¹) was calculated as (energy density/discharge time) × 3600.

Computational method

The structure of the PI and PC polymers is truncated to a simple monomer structure that is composed of naphthalene-tricarboxylic diimide (NDI) substituted with a -CH₃ group at the nitrogen position and a catecholate (CAT) moiety, respectively. The lithium, zinc and aluminum cations are considered to have their first coordination sphere filled with 4, 6 and 6 explicit water molecules, respectively. The binding free energies of the solvated metal cations are calculated with respect to the reduced form of the catecholate/imide monomer moieties from the following equation: $[\text{MON}]^{2-} + y[\text{M}(\text{H}_2\text{O})_x]^{m+} \rightarrow [\text{MON}-\text{M}_y(\text{H}_2\text{O})_{nx-z}]^{y^{m-2}} + z(\text{H}_2\text{O})$, where MON is the catecholate or imide species. The absolute redox potentials are calculated from: $E = -\Delta G_{\text{rxn}}/(2F)$, where ΔG_{rxn} is the free energy change for the 2e⁻-reduction reaction: $[\text{MON}] + 2e^- + y[\text{M}(\text{H}_2\text{O})_x]^{m+} \rightarrow [\text{MON}-\text{M}_y(\text{H}_2\text{O})_{nx-z}]^{y^{m-2}} + z(\text{H}_2\text{O})$. Full details of the computational protocol are presented in the ESI† and are taken from our previous work.⁴¹

Results and discussion

Effect of charge carriers on the electrochemical response

Redox response of individual electrodes with Li⁺, Zn²⁺, and Al³⁺ as charge carriers. The redox reactions in both anode and cathode redox polymers were probed by cyclic voltammetry (CV)

in a three-electrode cell using aqueous electrolytes containing different charge carriers, such as Li⁺, Zn²⁺ and Al³⁺. The poly(imide) (PI) anode (see Fig. 1a for the chemical structure) in the Li⁺ containing aqueous electrolyte demonstrated two successive redox processes with average peak potentials, $E_{1/2}$ ($[E_{\text{p,a}} + E_{\text{p,c}}]/2$) located at $E_{\text{PI},1} \approx -0.26$ V and $E_{\text{PI},2} \approx -0.73$ V (Fig. 1b, top panel). These redox peaks correspond to the transformation of PI into PI⁻[Li⁺] and then into PI²⁻[2Li⁺] to give n-doped states through conjugated carbonyl groups with concomitant electroneutralization by Li⁺ during the reduction sweep (Fig. 1a).^{33,35,44-46} The reverse reaction occurs in the subsequent oxidation sweep with the expulsion of Li⁺ from the enolate sites. Therefore, the overall redox reaction of PI can be considered as a quasi-reversible two successive one-electron process with an average conversion potential of $E_{\text{ave PI, Li}^+} \approx -0.5$ V. Here the term E_{ave} ($[E_{\text{PI},1} + E_{\text{PI},2}]/2$) is just used as the average conversion potential for a two successive one-electron process with the purpose of representing the anticipated voltage output of the full-cell when coupled with a positive electrode and should not be confused with the usage of $E_{1/2}$. Interestingly, when the Li⁺ charge carriers were substituted by divalent Zn²⁺ and trivalent Al³⁺, the PI exhibited similar electrochemical features; however, the redox processes appeared at slightly more positive potentials, *i.e.*, $E_{\text{ave PI, Zn}^{2+}} \approx -0.47$ V and $E_{\text{ave PI, Al}^{3+}} \approx -0.40$ V (see Fig. 1a for the schematic representation and Fig. 1b for CVs).

On the other hand, the poly(catechol) cathode (PC) (see Fig. 1c for the chemical structure) featured a single redox process corresponding to an anodic peak of PC²⁻[2Li⁺, 1Zn²⁺ or 1Al³⁺] to PQ (PQ refers to poly(*ortho*-quinone) transformation) and a cathodic peak of PQ to PC²⁻[2Li⁺, 1Zn²⁺ or 1Al³⁺] conversions. The CVs in Fig. 1b evidenced the quasi-reversible nature of this two-Li⁺ (one-Zn²⁺ or one-Al³⁺) and two-electron process.⁴¹ Importantly, differently from the PI, the average peak potentials of PC were dramatically shifted positive (*i.e.*, $E_{\text{PC, Li}^+} \approx 0.1$ V, $E_{\text{PC, Zn}^{2+}} \approx 0.28$ V, and $E_{\text{PC, Al}^{3+}} \approx 0.51$ V), in the

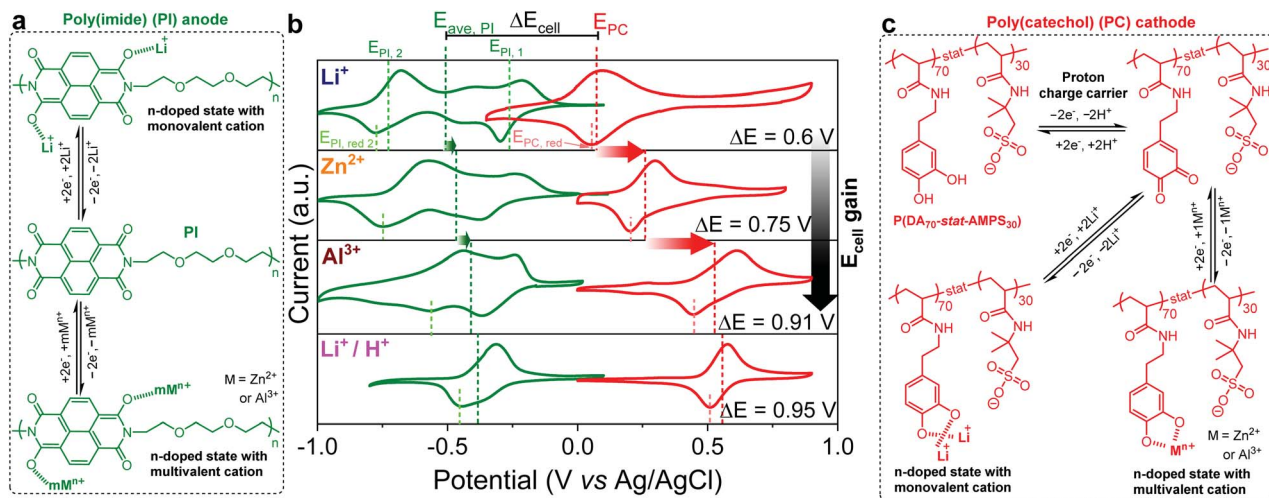


Fig. 1 (a and c) Schematic representation of the n-type redox behavior of PI (a) and PC (c) with both mono- and multivalent cations. (b) Cyclic voltammograms of PI (profiles in green) and PC (profiles in red) half-cells in unbuffered aqueous electrolytes containing different charge carriers, *i.e.*, Li⁺, Zn²⁺, Al³⁺, and Li⁺/H⁺ (top to bottom). The CVs were recorded at 10 mV s⁻¹ in a standard three-electrode configuration.



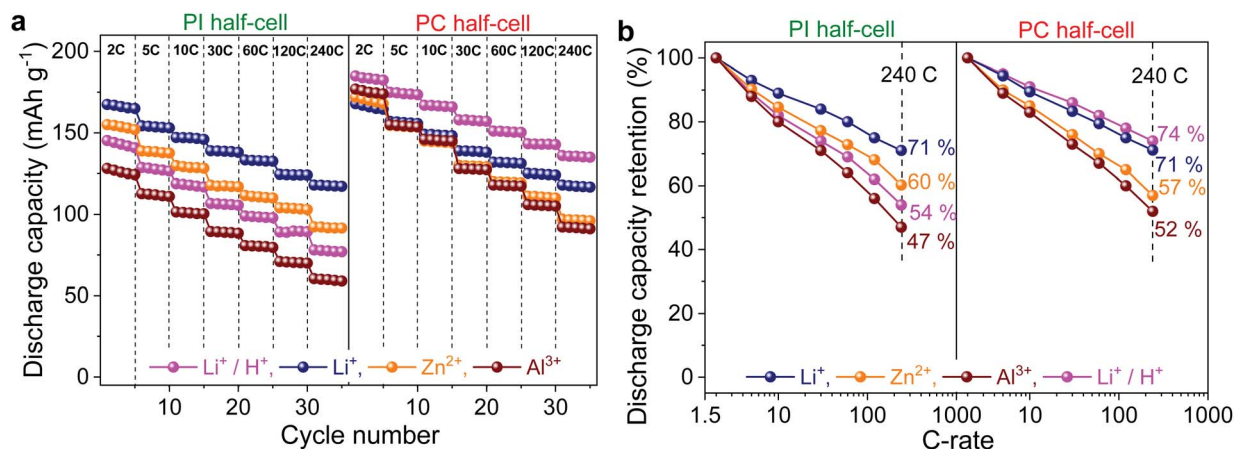


Fig. 3 (a) Discharge capacity vs. cycle number at increasing C-rates. (b) Discharge capacity retention at different C-rates. The discharge capacities at higher C-rates are normalized with respect to the discharge capacity at 2C (1C = 166 and 180 mA g⁻¹ for PI and PC, respectively).

Remarkably, even at a very high C-rate of 240C, PI and PC still retained 71, 60 and 47% and 71, 57 and 52% of their initial capacities in Li⁺, Zn²⁺ and Al³⁺, respectively. Additionally, both the electrode partners of the all-organic cell also demonstrated excellent dynamic performance in the Li⁺/H⁺ electrolyte, but the overall performance of PC was superior to that of PI (Fig. 3).

In order to understand the origin of the outstanding rate performance of PI and PC, the electrochemical kinetics of redox

reactions in polymer working electrodes were investigated by CV at different scan rates (v) in the aqueous electrolyte containing Li⁺ as the representative charge carrier. The Laviron method was used to determine the transfer coefficient (α) and apparent reaction rate constant (k^0) parameters (Fig. 4a, d and S6†).⁶⁴ The value of α was close to 0.5 for both systems, indicating almost symmetric energy barriers for the oxidation and reduction reactions. Furthermore, the calculated k^0 was found

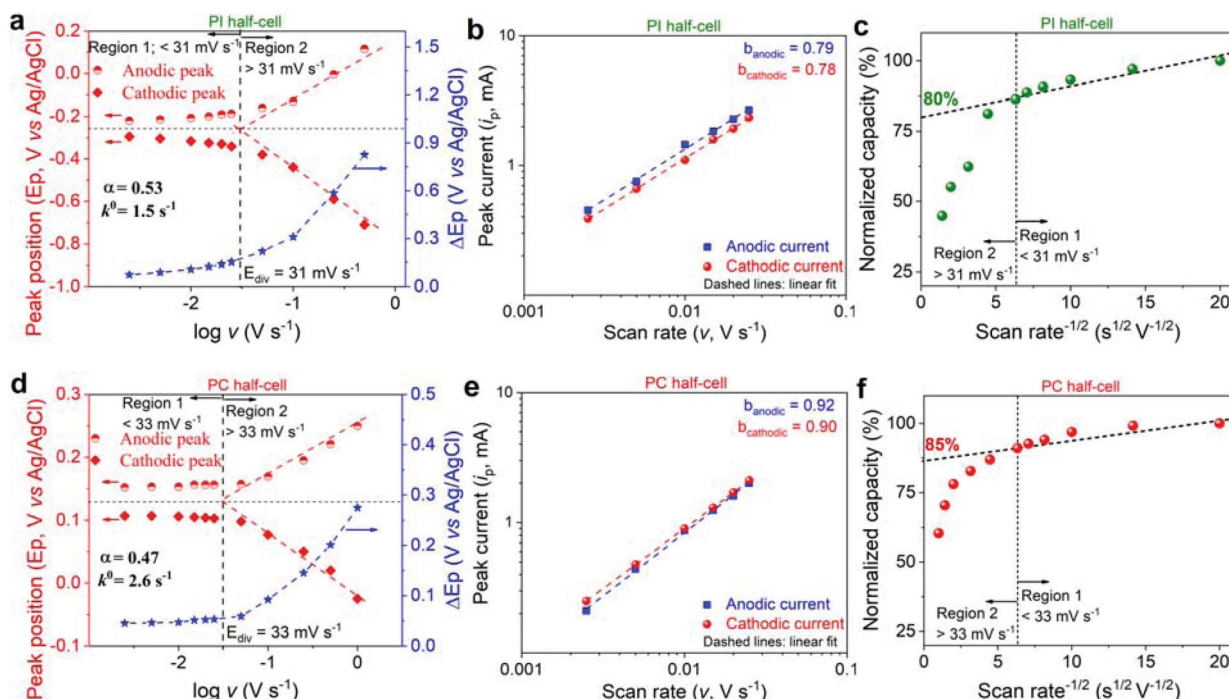


Fig. 4 Kinetic evaluation of PI and PC half-cells. (a and d) Laviron plots, indicating the variation of anodic and cathodic peak positions (E_p), and ΔE_p as a function of the scan rate on a logarithmic scale. (b and e) Plots of peak current vs. scan rate on a logarithmic scale. (c and f) Normalized capacity vs. scan rate^{-1/2} plots. The dashed vertical line in (a, c, d and f) separates two distinct kinetic regions: Region 1 below E_{div} where the capacity is mostly independent of the scan rate, and region 2 above E_{div} where the capacity is limited by semi-infinite linear diffusion. The y-intercept in Fig. 4c and f corresponds to the extrapolation of the infinite scan rate capacity (% capacity_{non-diffusion-controlled}). This dashed diagonal line is drawn based on the two distinct kinetic regions.



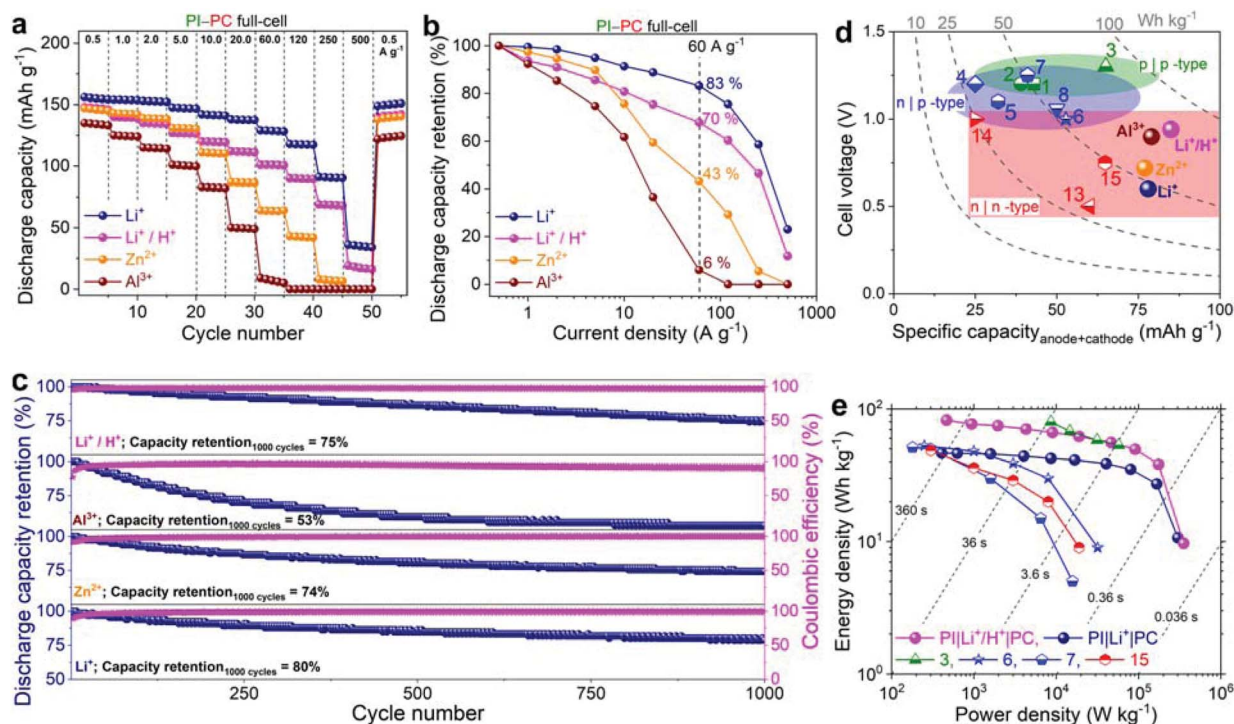


Fig. 5 (a and b) Rate performance of PI-PC full-cells: discharge capacity vs. cycle number at different current densities (a), and discharge capacity retention (b). (c) Cyclic performance: discharge capacity retention (%) and coulombic efficiencies measured at 5 A g^{-1} . The capacity and current density in experiments a–c were based on the PI component of the full-cell. (d and e) Comparison of full-cell performance with the state-of-the-art all-polymer aqueous stationary batteries: cell voltage vs. specific capacity (d) and Ragone plot (e). The specific capacity and gravimetric energy/power density were evaluated based on the total mass of the anode and cathode. Both these plots for various all-organic full-cells (mostly, all-polymer) are computed by considering some of the best performing full-cells in their class (see Table S1†). p|p-type: half-filled green symbols in the light green region, n|p-type: half-filled blue symbols in the light blue region, n|n-type: half-filled red symbols in the light red region, and filled spheres represent this work.

Zn^{2+} , Al^{3+} , and Li^+/H^+ , respectively (Fig. 5a). The rate performance of PI-PC full-cells is once again hampered in the $\text{Li}^+ < \text{Zn}^{2+} < \text{Al}^{3+}$ order, which is in accordance with the half-cell studies. For instance, when the applied current density was increased to 60 A g^{-1} , full-cells achieved discharge capacities of 129, 64, and 7 mA h g^{-1} , corresponding to 83, 43, and 6% of their initial capacities in Li^+ , Zn^{2+} , and Al^{3+} , respectively (Fig. 5b). Remarkably, full-cells in Li^+ and Li^+/H^+ can still deliver discharge capacities of 35 and 17 mA h g^{-1} , respectively, at even an extremely high current density of 500 A g^{-1} (corresponding to a sub-second charge or discharge), reflecting the unprecedented rate capabilities of both PI and PC in these electrolytes. Furthermore, when the current density was brought back to 0.5 A g^{-1} , nearly quantitative capacity recovery was observed in all the cases, discarding irreversible capacity fade during the high current experiments. It is also worth noting here that the average coulombic efficiencies were close to 100% in Li^+ and Zn^{2+} aqueous electrolytes at all the current densities, while slightly lower efficiencies (*ca.*, 94–97%) were obtained below 1 A g^{-1} with Al^{3+} and Li^+/H^+ and then subsequently improved to $> 99\%$ (Fig. S11†).

The cycling stability of PI-PC full-cells was evaluated at a current density of 5 A g^{-1} . Full-cells were able to maintain 80, 74, 53, and 75% of their initial capacities over 1000 GCD cycles

in Li^+ , Zn^{2+} , Al^{3+} , and Li^+/H^+ , respectively (Fig. 5c and S12†). Additionally, the coulombic efficiencies were stabilized at $>99\%$ after the initial few catechol-to-*ortho*-quinone activation cycles.

Finally, to demonstrate the availability of our PI-PC full-cells as sustainable high-performance energy storage systems, we compared their performance with that of the state-of-the-art all-polymer aqueous stationary batteries. The maximum attained specific capacities in the range of $78\text{--}85 \text{ mA h g}^{-1}$ were higher than that of the reported AqPBs, and the average cell voltage of 0.95 V in Li^+/H^+ was also notable for the n|n-type configuration (Fig. 5d and Table S1†). As shown in the Ragone plot (Fig. 5e), full-cells in Li^+ and Li^+/H^+ containing aqueous electrolytes can deliver a maximum energy/power density of $46.5 \text{ W h kg}^{-1}/302 \text{ kW kg}^{-1}$ and $82.2 \text{ W h kg}^{-1}/355 \text{ kW kg}^{-1}$, respectively. The concurrent high specific capacity, high cell voltage, and ultra-fast kinetics, particularly in the mixed Li^+/H^+ aqueous electrolyte, endowed the PI-PC full-cell with a steady and high energy density over a wide range of power values that clearly rivals most of the state-of-the-art AqPBs, and also comparable to the poly(viologen)-poly(2,2,6,6-tetramethylpiperidinyloxy-4-yl acrylamide) aqueous battery (example 3 in Fig. 5e and Table S1†),²⁸ which is based on the p|p-type combination. Yet another advantage of n|n-type combination is that it can make use of lighter weight shuttling cations (*e.g.*, H^+ , Li^+ *etc.*), in contrast to



the p|p- and n|p-type configurations, which require bulky anions and dual ions, respectively, as the electroneutralizing charge carriers. Consequently, when the energy and power density were evaluated based on the total mass of both electrodes and the consumed salt, a small decrease of energy/power density (<1%) was noted for PI–PC full-cells in Li^+ and Li^+/H^+ , while a substantial lowering of 19, 32, and 30% energy/power density for the examples 3,²⁸ 6,³⁰ and 7,³³ respectively, is noticeable from their corresponding Ragone plots (Fig. 5e, S13 and Table S1†).

Conclusions

In this work, we have developed all-organic aqueous batteries comprising a poly(imide) (PI) anode and poly(catechol) (PC) cathode that demonstrated tunable electrochemical performance. We realized this by exploiting the distinctive strength of metal cation–redox core ionic interactions of electrode partners with different charge carriers based on their n-type redox behavior, resulting in various cationic rocking-chair cells. The increase of cell voltage from 0.58 to 0.74 and further to 0.89 V was achieved, when the type of charge carrier changed from Li^+ to Zn^{2+} and to Al^{3+} . Adversely, this gain also comes with the penalty of rate capability and cycling stabilities in the $\text{Li}^+ < \text{Zn}^{2+} < \text{Al}^{3+}$ order. The PI–PC full-cell also worked in hybrid-ion mode with a mixed Li^+/H^+ aqueous electrolyte, exhibiting the highest cell voltage of 0.95 V with good cycling stability and excellent rate capability. The concurrent high specific capacity (85 mA h g^{-1}), high cell voltage (0.95 V), and ultrafast kinetics (working at 500 A g^{-1} , which corresponds to 0.1 s charge or discharge), particularly in Li^+/H^+ , provided an impressive energy density of ~ 80.6 W h kg^{-1} , where a high value of ~ 10 W h kg^{-1} was still achieved at an unprecedented power density of ~ 348 kW kg^{-1} based on the total mass of both electrodes and the consumed salt. This overall performance is far superior to that of most of the reported all-polymer aqueous stationary batteries.

Based on the CV, GCD results and DFT calculations, we postulate that PI and PC can be used as universal organic electrodes in numerous Li-ion and post-Li-ion energy storage technologies, including proton and all-polymer batteries, stemming from their versatile n-type charge storage mechanism. The development of such universal organic electrodes is particularly intriguing and gaining popularity among the battery community due to the fact that it demands minimal electrode/device engineering efforts. We hypothesize that the combination of high safety aqueous electrolytes and high-performance PI and PC based organic electrodes could offer a practical option as a truly sustainable energy storage system for wide use in large-scale applications.

Conflicts of interest

The authors declare no conflict of interest.

Acknowledgements

RM, NP and AM thank the Spanish Ministry of Science, Innovation and Universities through the SUSBAT project

(Ref. RTI2018-101049-B-I00) (MINECO/FEDER, UE) and the European Research Council (ERC) through the “MFreeB” project (grant agreement No. 726217) for financial support. NP also appreciates Spanish MINECO for the Juan de la Cierva formation fellowship [FJC2018-037781-I] received to carry out this work. AM acknowledges the TALENTO grant (2017-T1/AMB-5264) from the Comunidad de Madrid for financial support. The authors acknowledge the computing facilities of CSUC for providing resources that contributed to the research results reported within this paper. DM and NC are grateful to the financial support of the European Research Council by the Proof of Concept Grant Innovative Polymeric Batteries by 3D Printing (iPes-3DBat) 789875. CD and CJ thank the “Fonds de la Recherche Scientifique” (FRS-FNRS) for funding.

Notes and references

- Z. Yang, J. Zhang, M. C. W. Kintner-Meyer, X. Lu, D. Choi, J. P. Lemmon and J. Liu, *Chem. Rev.*, 2011, **111**, 3577–3613.
- S. Chu, Y. Cui and N. Liu, *Nat. Mater.*, 2017, **16**, 16–22.
- M. Li, J. Lu, Z. Chen and K. Amine, *Adv. Mater.*, 2018, **30**, 1800561.
- K. Turcheniuk, D. Bondarev, V. Singhal and G. Yushin, *Nature*, 2018, **559**, 467–470.
- H. Kim, J. Hong, K.-Y. Park, H. Kim, S.-W. Kim and K. Kang, *Chem. Rev.*, 2014, **114**, 11788–11827.
- J. Huang, Z. Guo, Y. Ma, D. Bin, Y. Wang and Y. Xia, *Small Methods*, 2019, **3**, 1800272.
- R. Demir-Cakan, M. R. Palacin and L. Croguennec, *J. Mater. Chem. A*, 2019, **7**, 20519–20539.
- P. Novák, K. Müller, K. S. V. Santhanam and O. Haas, *Chem. Rev.*, 1997, **97**, 207–282.
- S. Muench, A. Wild, C. Friebe, B. Häupler, T. Janoschka and U. S. Schubert, *Chem. Rev.*, 2016, **116**, 9438–9484.
- J. Kim, J. H. Kim and K. Ariga, *Joule*, 2017, **1**, 739–768.
- S. Lee, G. Kwon, K. Ku, K. Yoon, S.-K. Jung, H.-D. Lim and K. Kang, *Adv. Mater.*, 2018, **30**, 1704682.
- K. Amin, L. Mao and Z. Wei, *Macromol. Rapid Commun.*, 2019, **40**, 1800565.
- J. Xie and Q. Zhang, *Small*, 2019, **15**, 1805061.
- Y. Y. Lai, X. Li and Y. Zhu, *ACS Appl. Polym. Mater.*, 2020, **2**(2), 113–128.
- N. Casado, D. Mantione, D. Shanmukaraj and D. Mecerreyes, *ChemSusChem*, 2019, **13**(9), 2464–2470.
- Y. Chen, S. Zhuo, Z. Li and C. Wang, *EnergyChem*, 2020, 100030.
- P. Poizot, J. Gaubicher, S. Renault, L. Dubois, Y. Liang and Y. Yao, *Chem. Rev.*, 2020, **120**(14), 6490–6557.
- P. Poizot, F. Dolhem and J. Gaubicher, *Curr. Opin. Electrochem.*, 2018, **9**, 70–80.
- C. Friebe, A. Lex-Balducci and U. S. Schubert, *ChemSusChem*, 2019, **12**, 4093–4115.
- J. Winsberg, T. Hagemann, T. Janoschka, M. D. Hager and U. S. Schubert, *Angew. Chem., Int. Ed.*, 2017, **56**, 686–711.
- D. P. Tabor, R. Gómez-Bombarelli, L. Tong, R. G. Gordon, M. J. Aziz and A. Aspuru-Guzik, *J. Mater. Chem. A*, 2019, **7**, 12833–12841.



